***Editor's note*: This ESI for article DOI: 10.1039/D0TA10136B was republished on 23rd February 2021, to fix errors in Tables S2 and S4 and Fig. S10.**

Supporting Information

Design of Phosphorus-Functionalized MXenes for Highly Efficient Hydrogen Evolution Reaction

Youchao Kong‡[a], Shanshan Yan‡[a], Jinxian Feng[a], Shuangpeng Wang[ab], and Hui Pan*[ab]*

[a]*MOE Joint Key Laboratory, Institute of Applied Physics and Materials Engineering, University of Macau, Macao SAR, 999078, P. R. China*

[b]*Department of Physics and Chemistry, Faculty of Science and Technology, University of Macau, Macao SAR, 999078, P. R. China*

Corresponding Authors

Hui Pan: huipan@um.edu.mo (email), 853-88224427 (tel.), 853-88222454 (fax).

Shuangpeng Wang: spwang@um.edu.mo (email).

‡These authors contributed equally to this work.

CONTENTS

Part1: Additional basic properties of predicted M_2CP_2.

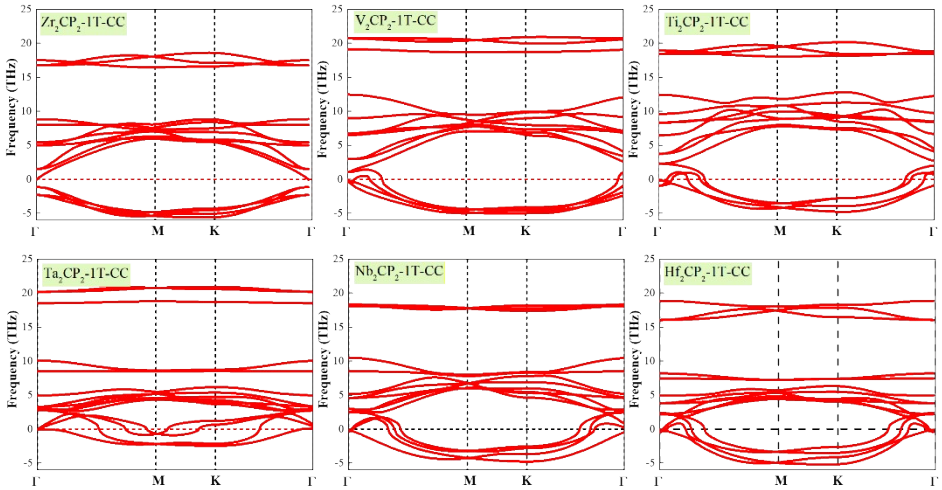

Figure S1| Calculated phonon dispersions of predicated M_2CP_2-1T-CC systems along high symmetry directions (Γ-M-K-Γ) of the Brillouin zone.

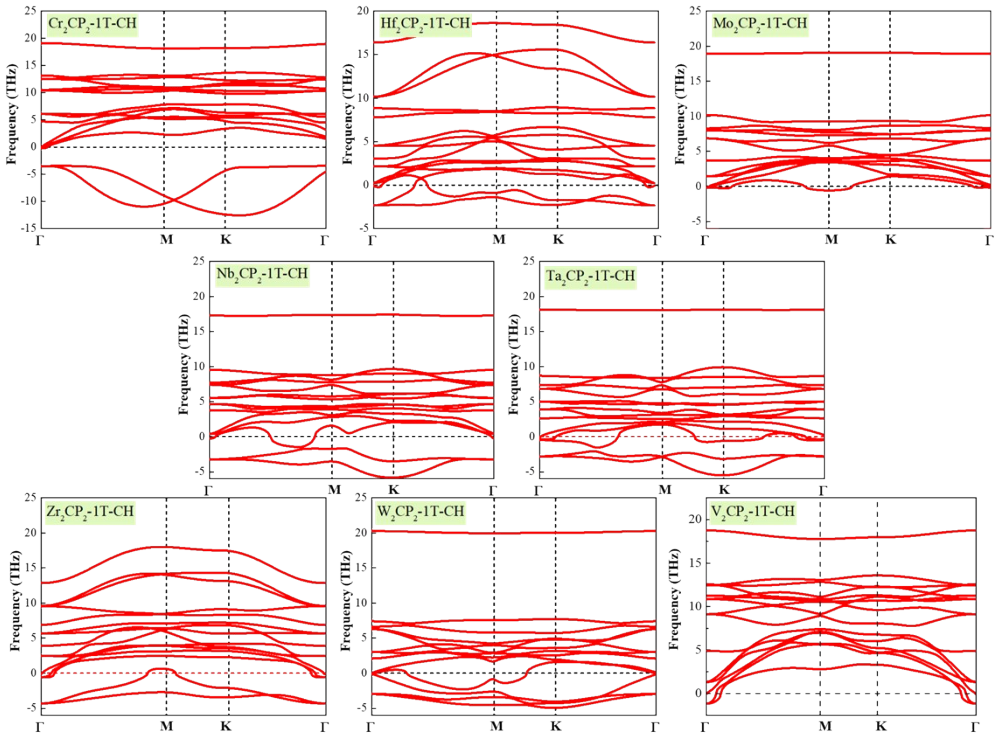

Figure S2| Calculated phonon dispersions of predicated M_2CP_2-1T-CH systems along high symmetry directions (Γ-M-K-Γ) of the Brillouin zone.

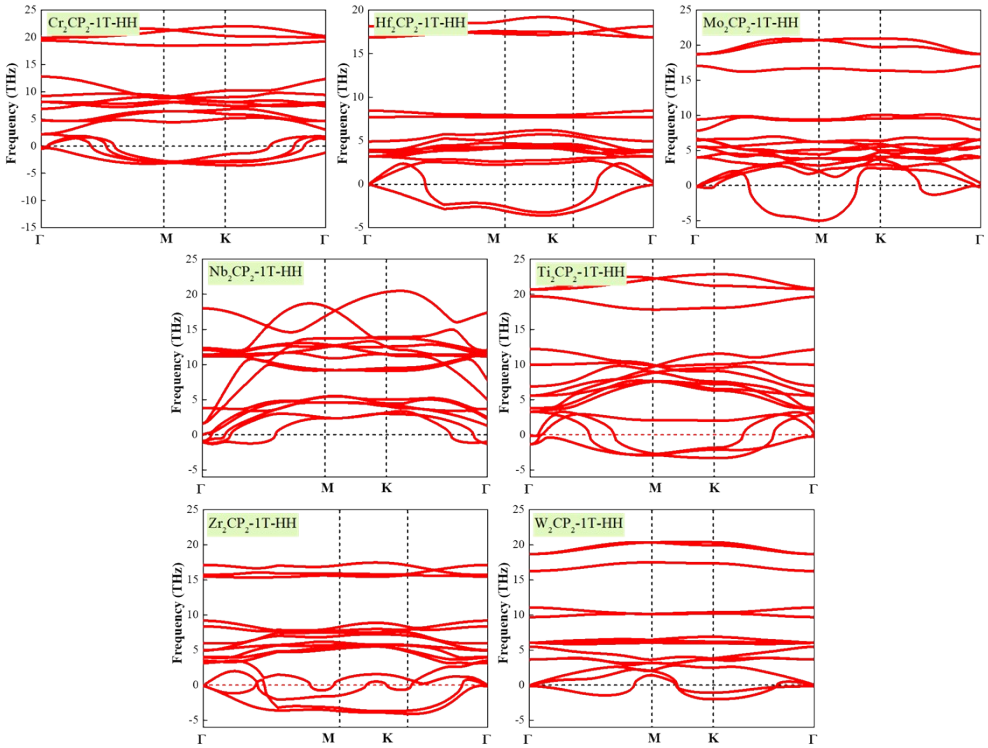

Figure S3| Calculated phonon dispersions of predicated M_2CP_2-1T-HH systems along high symmetry directions (Γ-M-K-Γ) of the Brillouin zone.

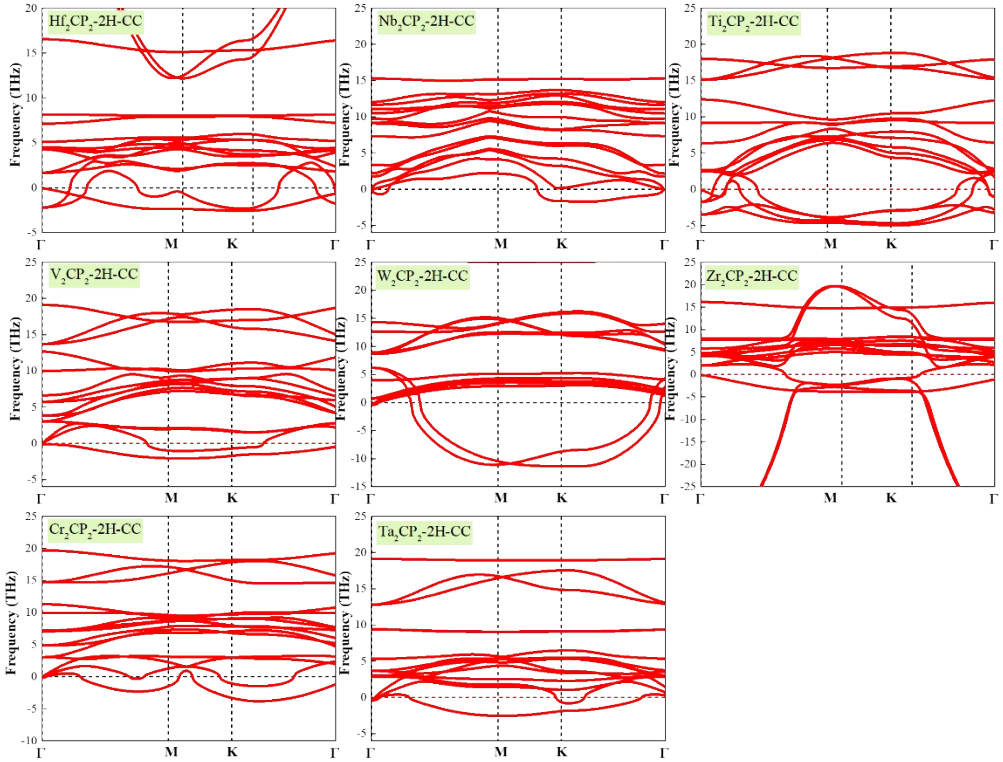

Figure S4| Calculated phonon dispersions of predicated M_2CP_2-2H-CC systems along high symmetry directions (Γ-M-K-Γ) of the Brillouin zone.

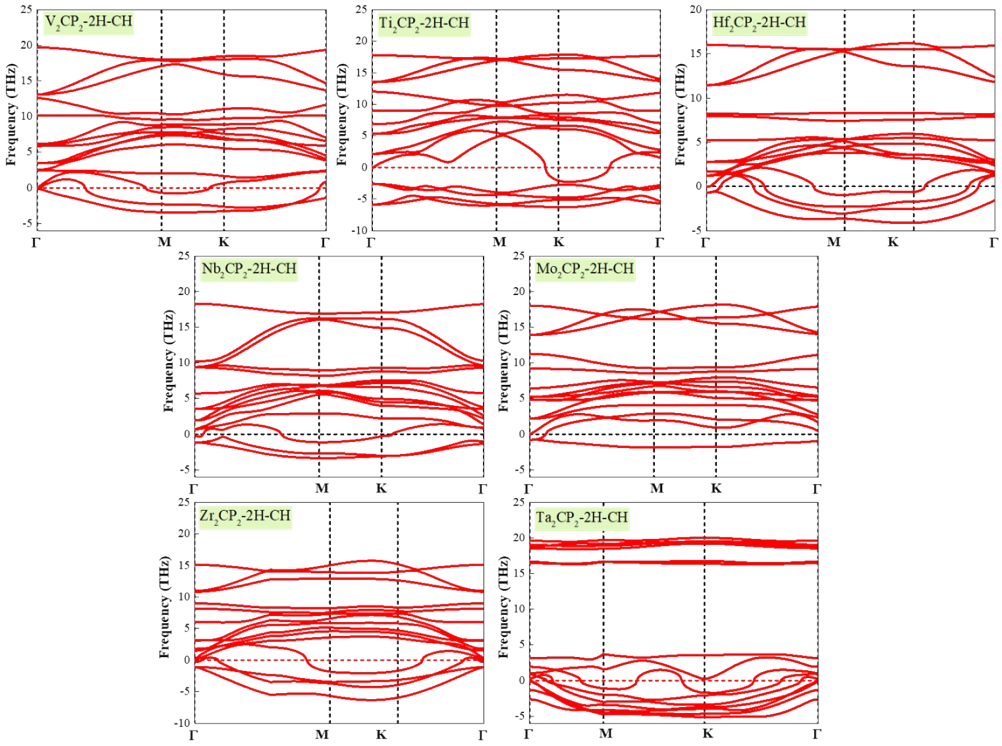

Figure S5| Calculated phonon dispersions of predicated M_2CP_2-2H-CH systems along high symmetry directions (Γ-M-K-Γ) of the Brillouin zone.

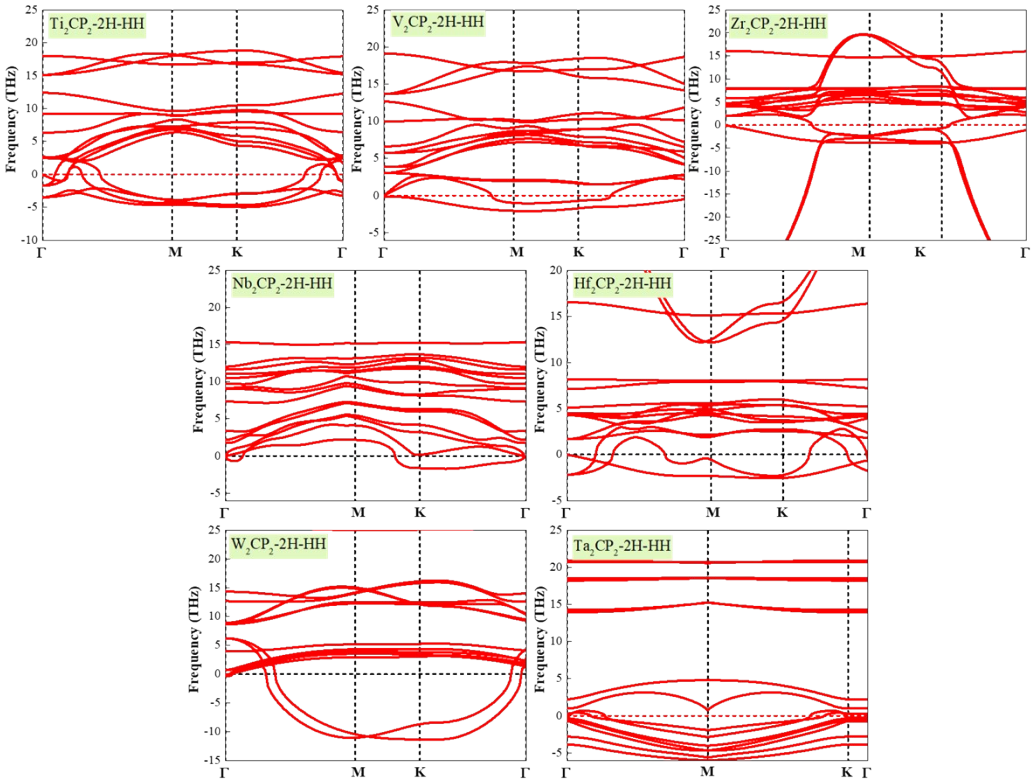

Figure S6| Calculated phonon dispersions of predicated M_2CP_2-2H-HH systems along high symmetry directions (Γ-M-K-Γ) of the Brillouin zone.

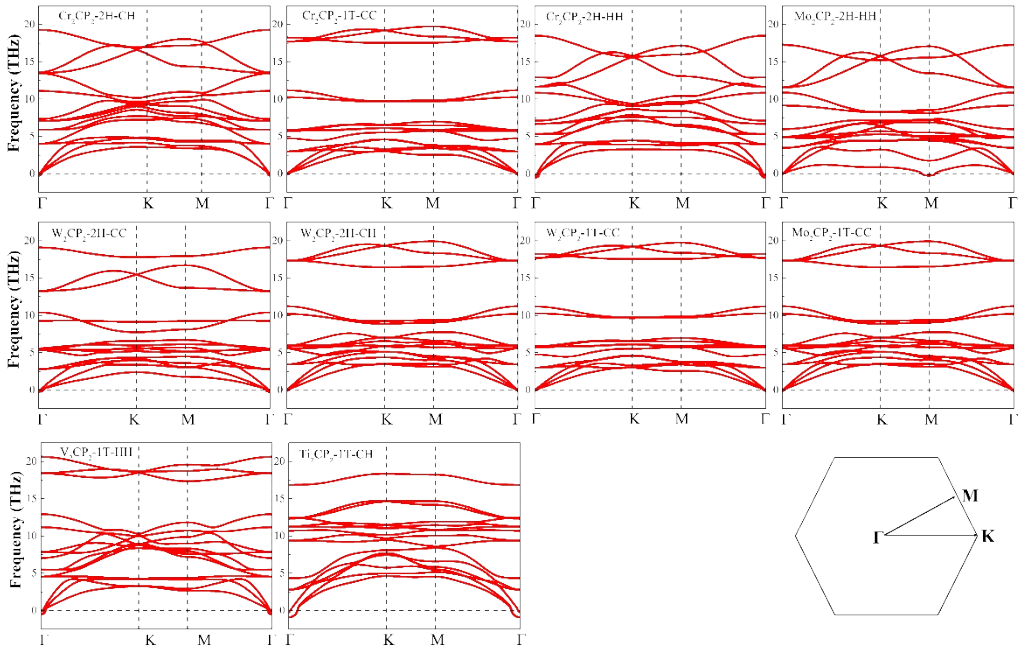

Figure S7| Calculated phonon dispersions of predicated stable M_2CP_2 systems along high symmetry directions (Γ-M-K-Γ) of the Brillouin zone.

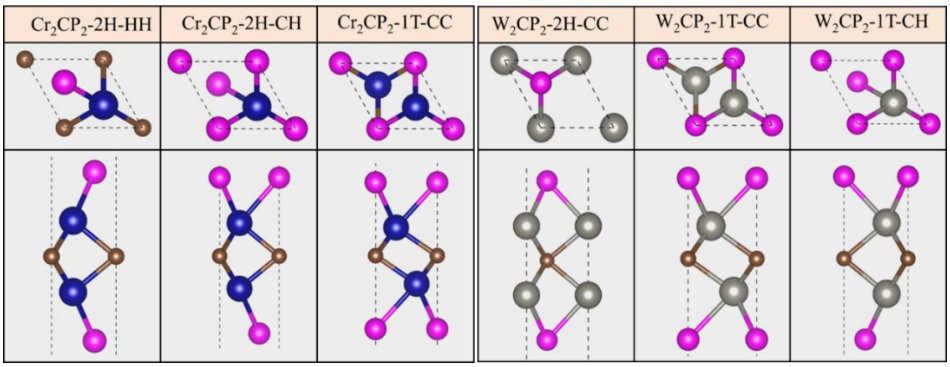

Figure S8| Optimized structures of predicted stable M_2CP_2 monolayers: Cr_2CP_2, W_2CP_2.

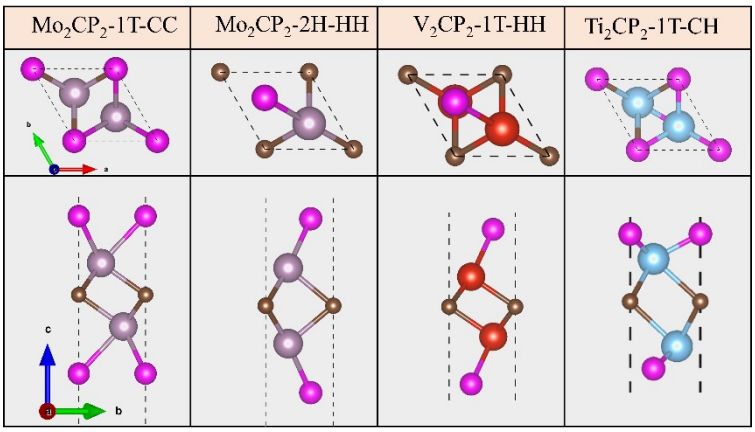

Figure S9| Optimized structures of predicted stable M_2CP_2 monolayers: Mo_2CP_2, V_2CP_2, Ti_2CP_2.

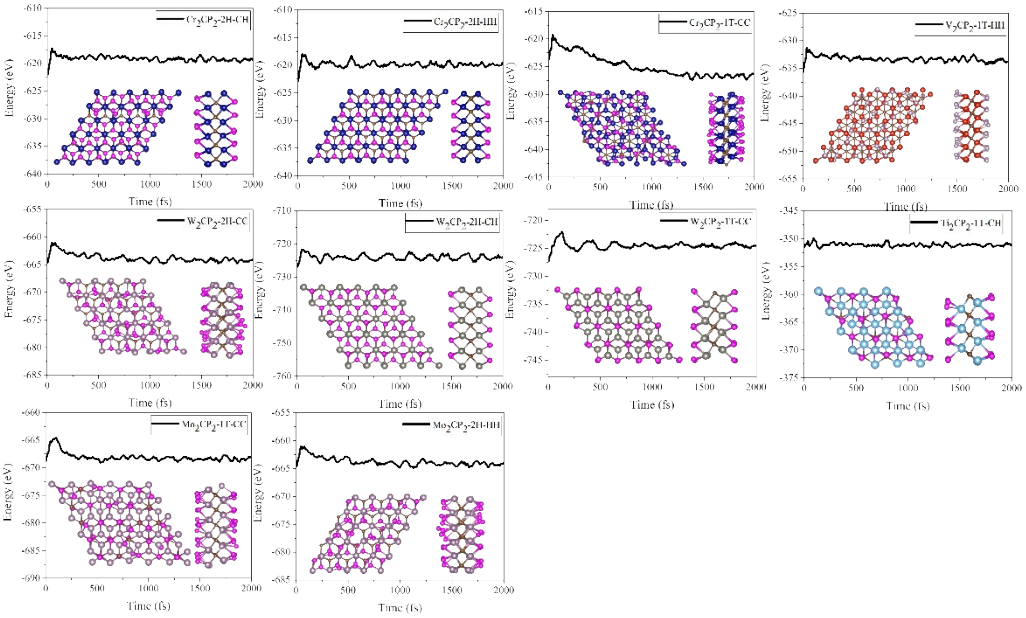

Figure S10| Energy evolution as the function of time in the AIMD simulation at room temperature. The timespan is 2ps. The insets are snapshots of atomic configurations at the end of AIMD simulations.

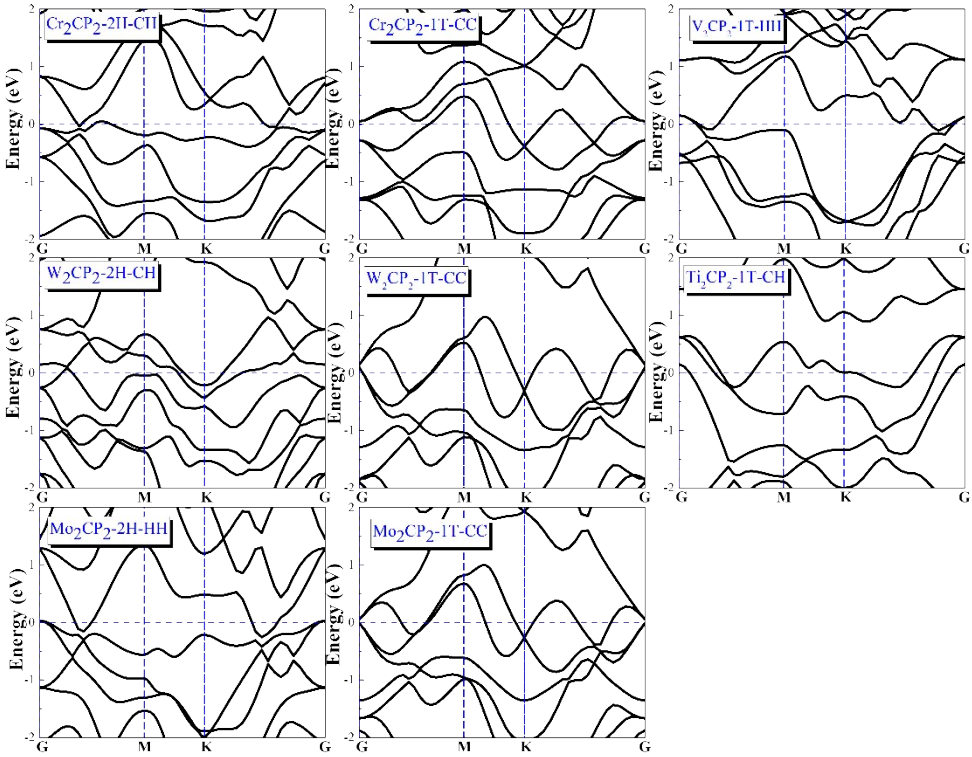

Figure S11| Band structures of non-magnetic M_2CP_2 monolayers.

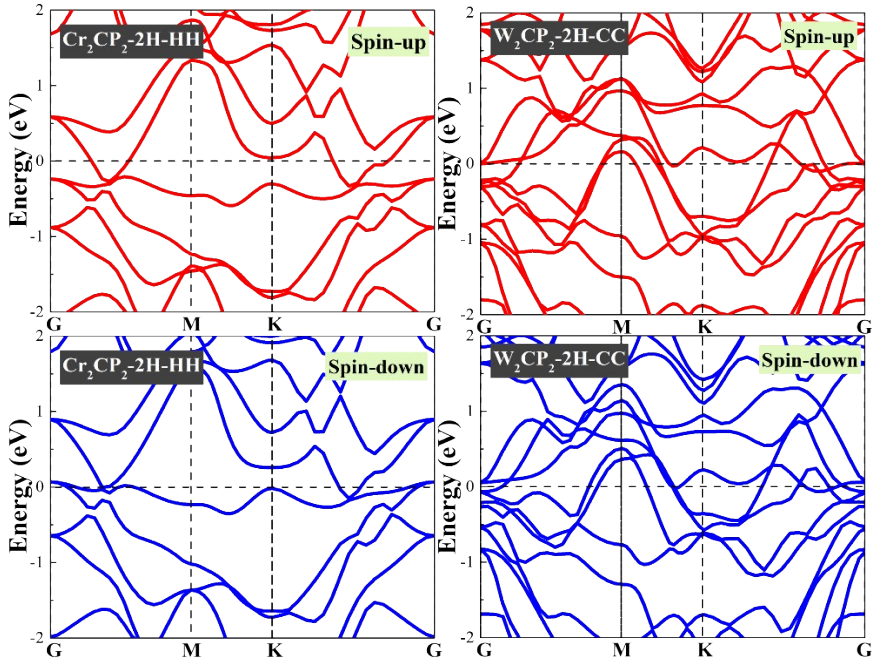

Figure S12| Spin down and spin-up band structures of magnetic M_2CP_2 monolayers: Cr_2CP_2-2H-HH and W_2CP_2-2H-CC.

Part2: Additional relation between ΔG_H and H coverage on M_2CP_2 monolayers

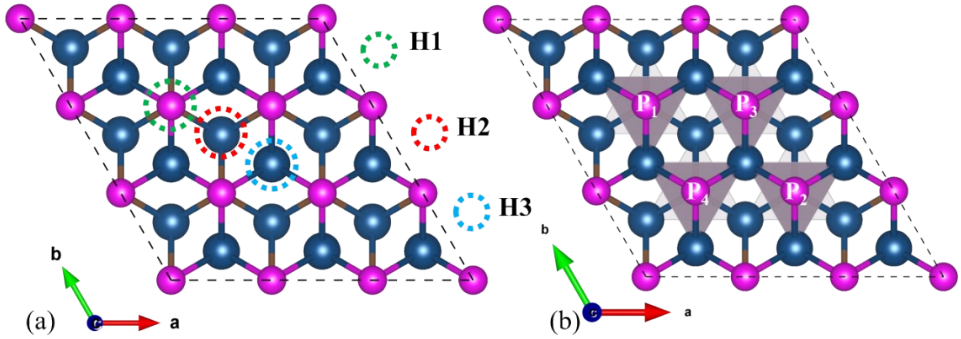

Figure S13| (a) Possible adsorption sites of H atom on the surface of M_2CP_2. (b) Coverage arrangement of H on the fixed area of M_2CP_2 monolayer.

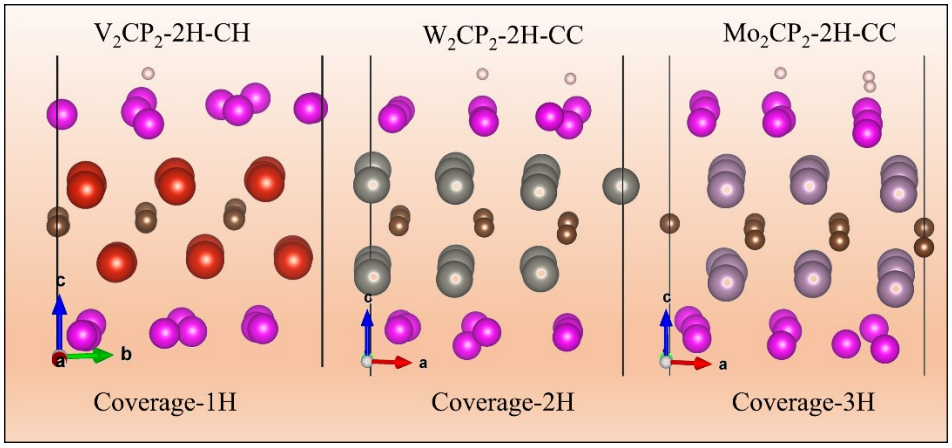

Figure S14| Serious surface distortion of M_2CP_2 when several H atoms absorbed on.

As reported, ΔG_H is not related to the binding energy between H and slab but also the coverage (numbers and arrangement) of H atoms on the active surface. Herein, we fixed the number of active sites for each M_2CP_2 monolayer by constructing a supercell with 3×3 unit cells. Then we calculate ΔG_H at different numbers of H and alignments. The corresponding coverage is from 1/9 to 4/9, the active sites named P1, P2, P3, P4 (**Figure S13b**). For one H atom, the four active sites are equal, while (P1+P2) ≠ (P1+P3) as two H atoms absorbed. Similarly, the (P1+P2+P3) ≠ (P1+P2+P4) for three H atoms, but only one combination of four H atoms on the limited surface of M_2CP_2 with a periodical boundary (**Figure S15**). According to these configurations, the possible adsorption pathways would be R1: P1→P12→P123→P1234; R2: P1→P12→P124→P1234; R3: P1→P13→P123→P1234; R4: P1→P13→P124→P1234 (**Figure S15**). The corresponding ΔG_H is calculated by manually adding H atoms.

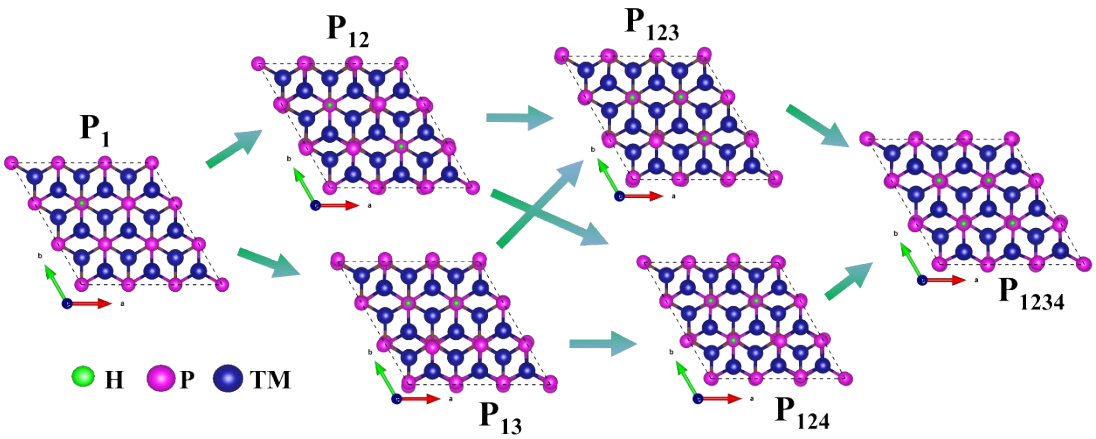

Figure S15| Possible configurations and pathways of H atoms adsorbed on the surface of M_2CP_2.

The calculated results display a diversity of HER performance responding to the coverage and arrangement of H atoms. Generally, the H adsorption ability of M_2CP_2 is steeply decreasing as the coverage increases, indicated by uphill Gibbs free energy from 1H to 4H. But the different structures will get to the fastest reaction at a specific point. For Cr_2CP_2 monolayer, the optimal ΔG_H is when coverage gets to (1/9,2/9), the corresponding value is within (-0.08,0.10 eV), which is closed to the Pt/C electrode. For Cr_2CP_2-1T-CC,2H-CH and 2H-HH, we find that surface symmetry has a limited effect on catalytic ability and the best HER locates at 2/9, 2/9, and 1/9, respectively. Compared with Cr (3d element)-based MXene, Mo-(4d element) and W-(5d element) based ones have stronger M-P bond, proved by Bader charge analysis (**Figure S16**). Then strong bond leads to a slow reaction at low H coverage (ΔG_H far away from 0 eV, **Figure S16d~f**). As H coverage increases, the reaction barrier gets to lower. The fastest HER for all W- and Mo-based MXene locates at 4/9, which is quite closed to the ideal condition (0 eV), the corresponding value is -0.01, -0.07, -0.06 eV for W_2CP_2-1T-CC, W_2CP_2-2H-CH, Mo_2CP_2-1T-CC, respectively. Last we consider the arrangement of H adsorbed, we find that nearly all M_2CP_2 prefer to the pathway of R4 (P1→P13→P124→P1234) (Blue line, **Figure S16**), except for the step 2H→3H of W_2CP_2- and Mo_2CP_2-1T-CC and W_2CP_2-2H-CH.

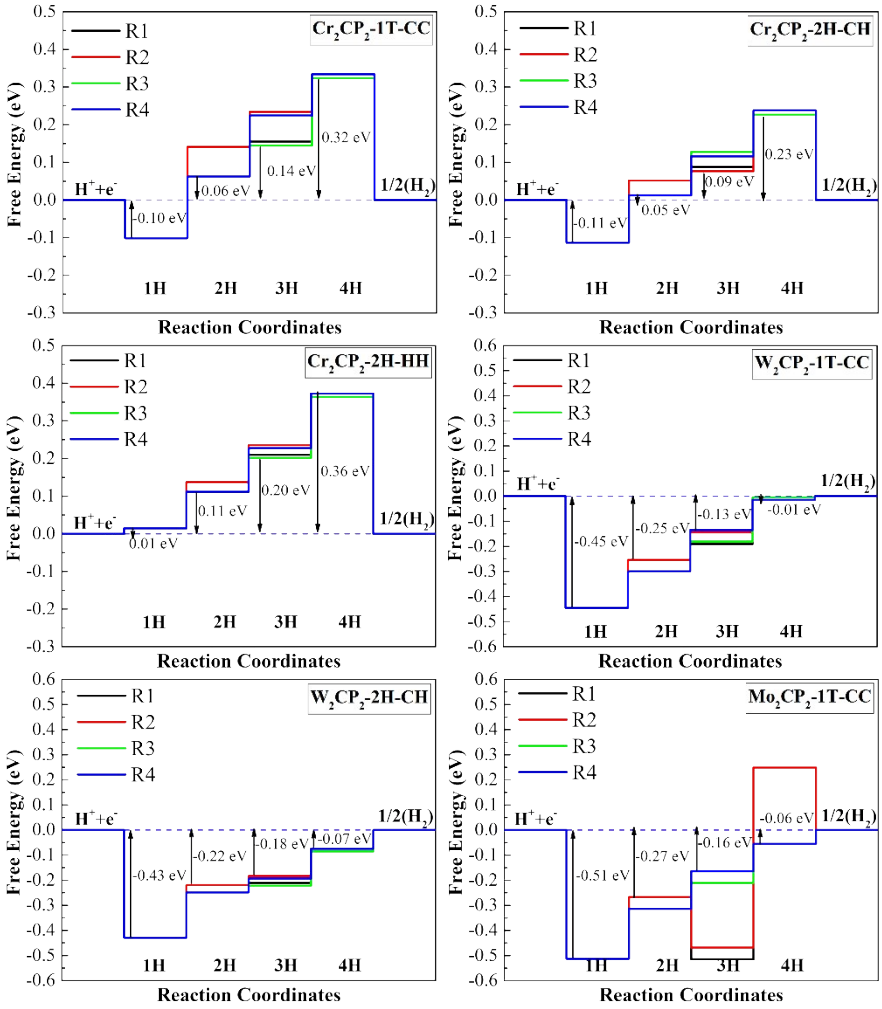

Figure S16| Bader charge transfer along with possible sequences and arrangements of the H adsorption on M_2CP_2 monolayers.

For a better understanding of the mechanism, the Bader charge of each step for M_2CP_2 is calculated (**Figure S17**). The average charge is defined as ($\rho_v = (\sum_n \rho_i)/n$), where ρ_i is the charge transfer from slab to P atom, and n is the number of hydrogen atoms. The Bader charge analysis exhibits: (1) 0.3~0.4 |e| is extracted from slab to P. (2) The value of charge transfer in the previous step would dramatically affect the HER performance in the next step. For example, in comparison with Cr_2CP_2-1T-CC, charge transfer of Cr_2CP_2-2H-CH along R3 is less than R2 at n(H)=2 (**Figure S17a&b**), leading an opposite trend of HER performance at n(H)=3 (**Figure S17a&b**).

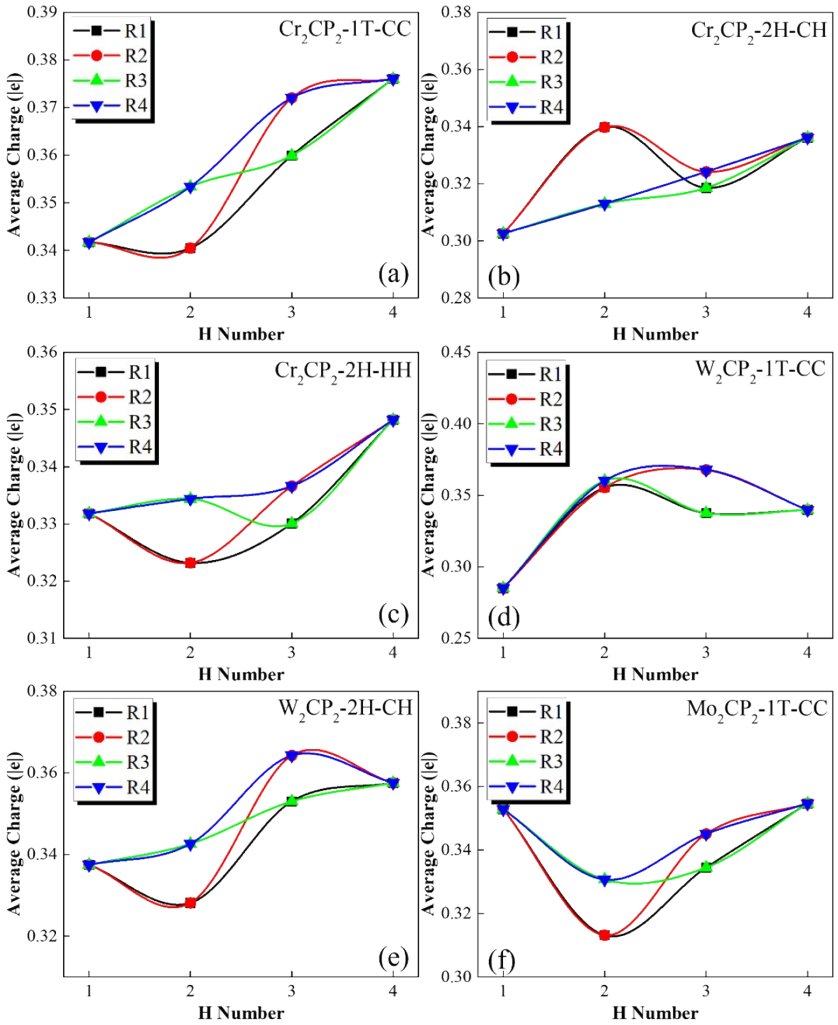

Figure S17| Bader charge transfer along various coverages of H atoms on surface of M_2CP_2.

The HER activity on P-MXene originates from the interaction between H atom and P atom. To further understand that how the HER activity varies on different P-functionalized MXenes. We divide P-MXenes into two groups: first group (Cr_2CP_2-1T-CC, Cr_2CP_2-2H-CH, W_2CP_2-1T-CC, and W_2CP_2-2H-CH) and second group (Cr_2CP_2-1T-CC, W_2CP_2-1T-CC, and Mo_2CP_2-1T-CC). The first group helps us understand how the symmetry could affect HER activity with the same formula. The other group is aimed to study how different metal atoms would impact the HER performance with the same symmetry. Since the Bader charge has been widely used for the qualitative analysis in electrocatalysis, we utilize it to give an explanation. The schematic structure and calculated charge transfer are shown in **Figure S18** and **Table S6**, respectively.

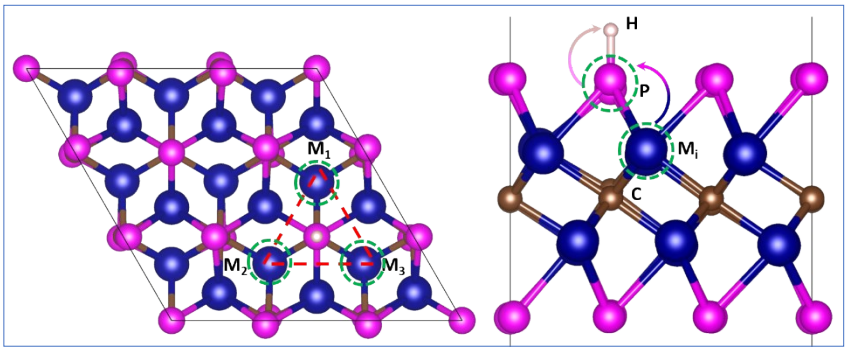

Figure S18| Schematic representation of the charge transfer on P-MXene.

We could find that M_i atoms nearby P atom work as an engine to provide stable charge to the P in M_2CP_2, leading to a negatively charge state, as indicated by the positive value of charge transfer without H atom covered on (**Table S6**). When one H atom attacks the P atom, the charge quickly moves from P to H atom. The P state turns to be positive. The transfer mount of charge is within (0.3, 0.4 |e|). In this process, the charge of M_i is nearly static.

For the first group, we found that same formula with different symmetry cannot dramatically affect the distribution of charge (e.g. P), leading to a similar HER activity. But for the second group, we noticed that M_2CP_2 with different metals in the same symmetry demonstrated significantly different charge. For example, the charge transfer of P atom is -0.083, -0.028 and -0.006 |e| for Cr_2CP_2-1T-CC, W_2CP_2-1T-CC, Mo_2CP_2-1T-CC, respectively. The corresponding Gibbs free energy is -0.10, -0.45, -0.51 eV, indicating that more charge injected into H atom would bring more active HER activity ($\Delta G \rightarrow 0$ eV). Besides, we believed that Heyrovsky process should be the main microkinetic activity on various P-MXenes at the optimal H coverage.

Part3: Additional HER evaluation from the microkinetic perspective.

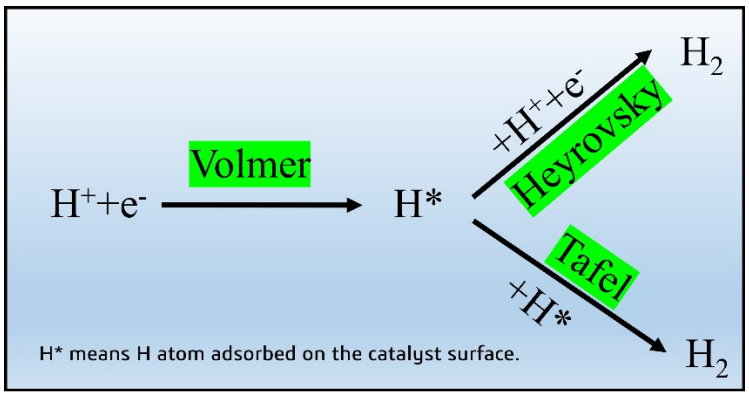

Figure S19| Schematic representation of mechanism of hydrogen evolution reaction.

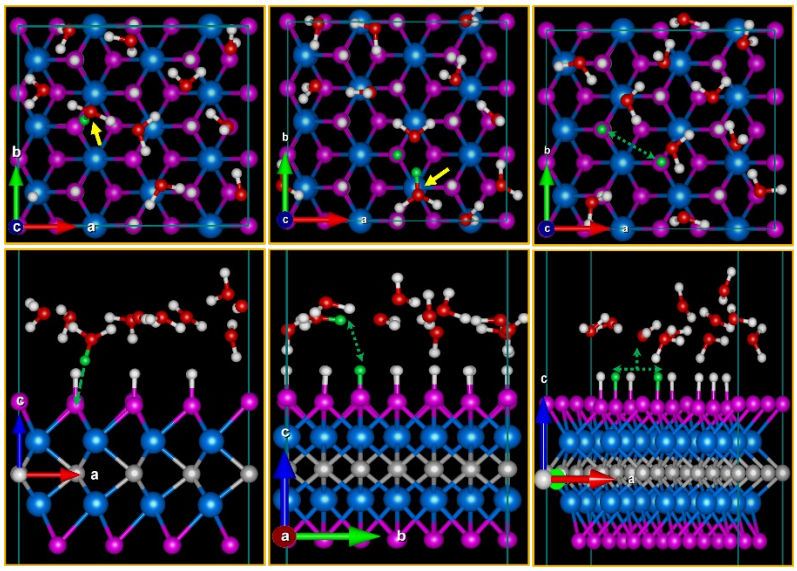

Figure S20| Model for the solved WCH system with hydrogen coverage of 8/12 as an example: Tafel step (left column), Heyrovsky step (middle column) and Tafel Step (right column). Green ball represents the proton or H* to react. H_3O^+ is indicated by yellow arrow.

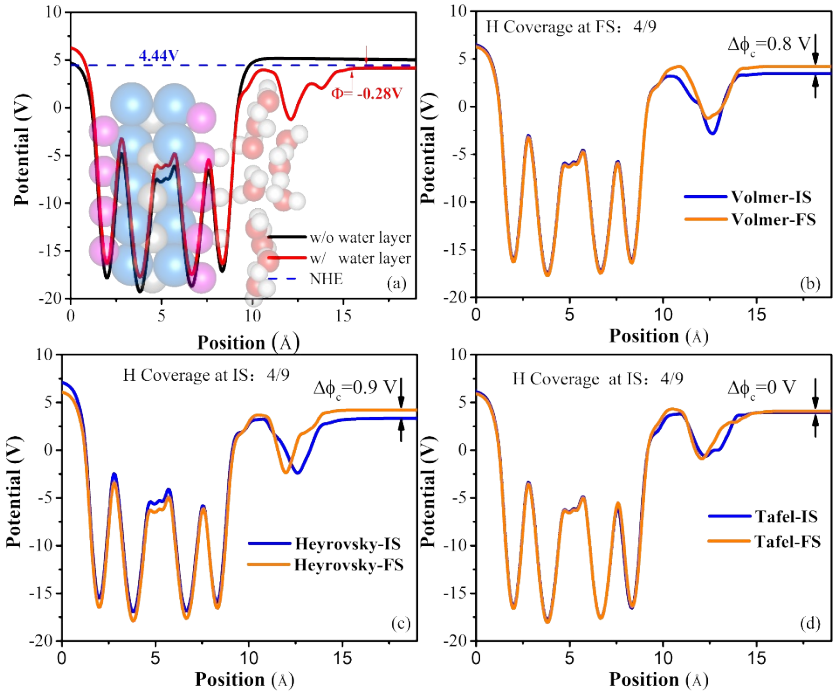

Figure S21| Electrostatic potential difference of WCH (a) with and without water layer; Electrostatic potential difference between initial state and final state in (b) Volmer, (c) Heyrovsky, and (d) Tafel process.

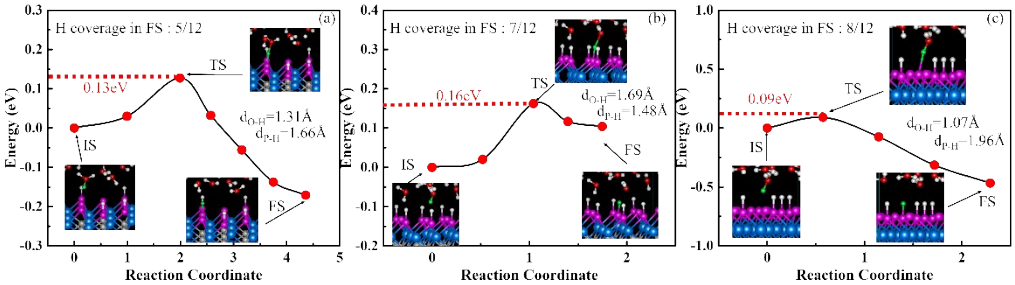

Figure S22| Minimum-energy pathway of Volmer reaction on WCH surface under the H coverage of 5/12 (a), 7/12 (b) and 8/12 (c) in finial state. Insets show side views of IS, TS and FS, where the transferred H is presented in green color.

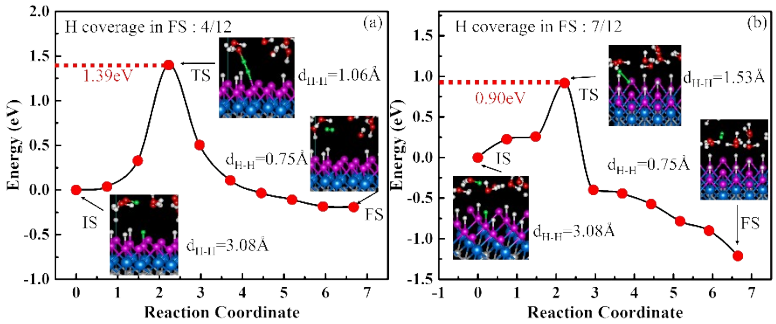

Figure S23| Minimum-energy pathway of Heyrovsky reaction on WCH surface under the H coverage of 4/12 (a) and 7/12 (b) in final state. Insets show side views of IS, TS and FS, where the transferred and energetic H* are presented in green color.

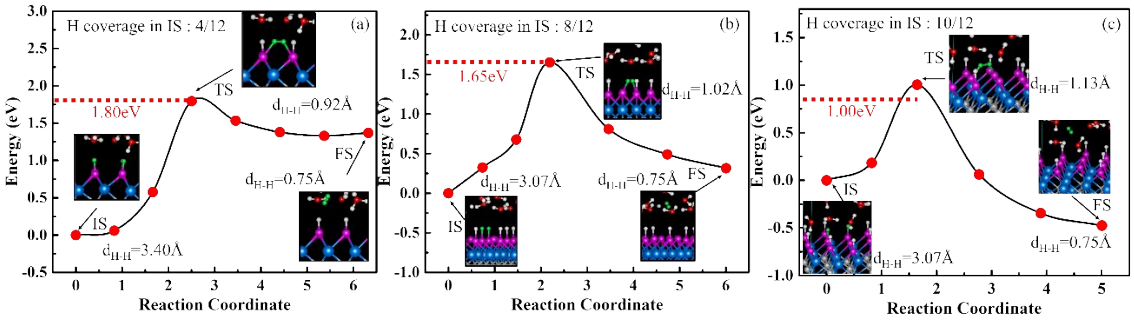

Figure S24| (a) Minimum-energy pathway of Tafel reaction on WCH surface under the H coverage of 4/12 (a), 8/12 (b), 10/12 (c) in initial state. Insets show side views of IS, TS and FS, where the energetic H* is presented in green color.

Part4: Additional Data Tables

Table S1| Structural parameters of predicated stable M_2CP_2 monolayers. d_{M-C} is the bond length of transition metal and carbon. d_{M-P} is the bond length of transition metal and phosphorus. ∠C-M-C is the angle of transition metal and neighboring carbons. ∠P-M-P is the angle of transition metal and neighboring phosphorus. E_f indicates the formation energy of M_2CP_2 from their precursors.

Structures	d_{M-C} (Å)	d_{M-P} (Å)	∠C-M-C (°)	∠P-M-P (°)	Magnetism/unit (μB)	E_f/unit (eV)
Cr_2CP_2-1T-CC	1.98	2.42	91.64	71.81	0	-3.23
Cr_2CP_2-2H-CH	2.05	2.39	83.80	63.94	0.059	-2.25
Cr_2CP_2-2H-HH	2.05	2.38	84.07	70.43	0.543	-2.31
Mo_2CP_2-1T-CC	2.15	2.54	89.78	73.15	0	-2.49
Mo_2CP_2-2H-HH	2.22	2.51	83.22	71.78	0	-2.10
Ti_2CP_2-1T-CH	2.32	1.91	79.80	99.66	0	**11.64**
V_2CP_2-1T-HH	2.04	2.47	91.62	72.36	0	-2.65
W_2CP_2-1T-CC	2.16	2.53	89.82	73.93	0	-2.62
W_2CP_2-2H-CC	2.22	2.51	83.70	72.19	0.476	-2.19
W_2CP_2-2H-CH	2.23	2.51	83.38	72.53	0	-2.44

Table S2| Summary of 54 M_2CP_2 monolayers and the corresponding energy per unit in stable phase. 'Y' and 'N' stand for the stable and unstable phase. The phase in background color represents the ground state.

M_2CP_2	1T Phase			2H Phase		
	C-C	C-H	H-H	C-C	C-H	H-H
Ti	N	Y	N	N	N	N
V	N	N	Y	N	N	N
Cr	Y -39.064	N	N	N	Y -38.874	Y -38.925
Zr	N	N	N	N	N	N
Nb	N	N	N	N	N	N
Mo	Y -41.924	N	Y	N	N	Y -41.577
Hf	N	N	N	N	N	N
Ta	N	N	N	N	N	N
W	Y -45.534	N	N	Y -45.332	Y -45.448	N

Table S3| Possible adsorption sites of H atom on the surface of M_2CP_2 monolayers and the corresponding adsorption energy.

Structures	Adsorption Sites	Adsorption Energy (eV)	Local Minimum?
Cr_2CP_2-1T-CC	H_1	-0.101	Yes
	H_2	1.283	No
	H_3	1.484	No
Cr_2CP_2-2H-CH	H_1	-0.113	Yes
	H_2	1.851	No
	H_3	1.748	No
Cr_2CP_2-2H-HH	H_1	0.014	Yes
	H_2	2.119	No
	H_3	1.763	No
Mo_2CP_2-1T-CC	H_1	-0.513	Yes
	H_2	0.850	No
	H_3	1.304	No
W_2CP_2-1T-CC	H_1	-0.445	Yes
	H_2	2.433	No
	H_3	1.433	No
W_2CP_2-2H-CH	H_1	-0.429	Yes
	H_2	1.407	No
	H_3	0.778	No

Table S4| Δ U changes with the coverage of H atoms on WCH surface at a fixed proton concentration.

Volmer	IS			FS			
Coverage in FS	Vacuum (eV)	Fermi (eV)	WF (eV)	Vacuum (eV)	Fermi (eV)	WF (eV)	ΔU
5/12	6.447	0.836	5.611	5.929	0.3125	5.616	0.005
6/12	5.928	0.795	5.133	5.885	0.3312	5.554	0.421
7/12	6.562	1.0991	5.463	6.638	1.133	5.505	0.042
8/12	6.638	1.133	5.505	6.454	0.9533	5.5007	-0.004

Heyrovsky	IS			FS			
Coverage in FS	Vacuum (eV)	Fermi (eV)	WF (eV)	Vacuum (eV)	Fermi (eV)	WF (eV)	ΔU
4/12	6.465	1.099	5.366	5.666	0.045	5.621	0.255
6/12	7.125	1.631	5.494	6.163	0.606	5.557	0.063
7/12	7.178	1.649	5.530	5.892	0.397	5.495	-0.034

Table S5| Comparison with HER performance on other typical 2D catalysts.

Materials	ΔG_H (eV)	E_a (eV)	Coverage	Reference
Ni-V_2CO_2	-0.01	--	1/4	1
1T-MoS2	-0.22	0.62	1/4	2
MoS_2/BP	-0.15	--	1/16	3
Mo_2CTx	0.048	--	--	4
Ti_3NCTx	-0.058	--	4/8	5
Ti_3C_2	-0.09	0.42	1/2	6
2H-MoS_2-edge	0.12	1.50	1/2	7
Pt (111)	0.09	0.40	7/6	8,9
M_2CP_2	-0.01	0.83	4/9	This work

Table S6| Calculated charge transfer on various P-MXenes at H coverage of 1/9.

Charge Transfer (|e|)	Cr_2CP_2-1T-CC		Cr_2CP_2-2H-CH		W_2CP_2-1T-CC		W_2CP_2-2H-CH		Mo_2CP_2-1T-CC	
	w/ H	w/o H	w/ H	w/o H	w/ H	w/o H	w/ H	w/o H	w/ H	w/o H
H	0.342	0.000	0.303	0.000	0.337	0.000	0.353	0.000	0.285	0.000
P	-0.083	0.280	-0.059	0.295	-0.028	0.369	-0.018	0.360	-0.006	0.328
M_1	-0.978	-0.951	-0.855	-0.853	-1.141	-1.120	-1.015	-1.008	-1.025	-1.006
M_2	-0.974	-0.966	-0.863	-0.845	-1.142	-1.121	-1.012	-1.006	-1.027	-1.008
M_3	-0.977	-0.966	-0.862	-0.847	-1.140	-1.106	-1.012	-0.998	-1.019	-0.999

REFERENCES

1. C. Ling, L. Shi, Y. Ouyang, Q. Chen and J. Wang, *Advanced science*, 2016, **3**, 1600180.
2. Q. Tang and D.-e. Jiang, *Acs Catalysis*, 2016, **6**, 4953-4961.
3. T. Liang, Y. Liu, Y. Cheng, F. Ma and Z. Dai, *ChemCatChem*, 2020, **12**, 2840-2848.
4. Z. W. Seh, K. D. Fredrickson, B. Anasori, J. Kibsgaard, A. L. Strickler, M. R. Lukatskaya, Y. Gogotsi, T. F. Jaramillo and A. Vojvodic, *ACS Energy Letters*, 2016, **1**, 589-594.
5. T. A. Le, Q. V. Bui, N. Q. Tran, Y. Cho, Y. Hong, Y. Kawazoe and H. Lee, *ACS Sustainable Chemistry & Engineering*, 2019, **7**, 16879-16888.
6. X. Yang, N. Gao, S. Zhou and J. Zhao, *Physical Chemistry Chemical Physics*, 2018, **20**, 19390-19397.
7. C. Tsai, K. Chan, J. K. Nørskov and F. Abild-Pedersen, *Surface Science*, 2015, **640**, 133-140.
8. P. Lindgren, G. Kastlunger and A. A. Peterson, *ACS Catalysis*, 2019, **10**, 121-128.
9. E. Skúlason, G. S. Karlberg, J. Rossmeisl, T. Bligaard, J. Greeley, H. Jónsson and J. K. Nørskov, *Physical Chemistry Chemical Physics*, 2007, **9**, 3241-3250.